chemosensors

MDPI

Article

Eco-Friendly Carbon Paste Sensor Modified with Multi-Walled Carbon Nanotubes, Cesium Chloride, and Sodium Dodecyl Sulfate for Ultra-Sensitive Voltammetric Detection of Levocabastine in Artificial Tears and Nasal Spray: A Promising Approach to Ocular Pharmacokinetic Studies

Shimaa A. Atty [1], Shereen M. Azab [1], Asmaa H. Ibrahim [1], Fatma A. Fouad [2], Mahmoud A. Tantawy [3,*], Suliman A. Almahmoud [3] and Mona A. Abdel Rahman [4]

[1] Pharmaceutical Chemistry Department, Egyptian Drug Authority, Giza 12561, Egypt
[2] Department of Pharmaceutical Analytical Chemistry, Faculty of Pharmacy, Al-Azhar University, Nasr City, Cairo 11751, Egypt; fatmafouad2304.el@azhar.edu.eg
[3] Department of Pharmaceutical Chemistry and Pharmacognosy, College of Pharmacy, Qassim University, Buraydah 51452, Saudi Arabia; s.almahmoud@qu.edu.sa
[4] Analytical Chemistry Department, Faculty of Pharmacy, October 6 University, 6 October City, Giza 12858, Egypt; mona.alkhateb89@gmail.com
* Correspondence: ma.omar@qu.edu.sa

Abstract

This work reports a novel, ultra-sensitive electroanalytical sensor based on a carbon paste electrode modified with multi-walled carbon nanotubes, cesium chloride, and sodium dodecyl sulfate (CPE/MWCNT-CsCl/SDS) for the determination of the antihistamine levocabastine (LC). The structural, morphological, and surface properties of the nanocomposite and modified electrode were thoroughly characterized. Cyclic voltammetry (CV) and square wave voltammetry (SWV) showed that combining MWCNTs and CsCl markedly enhanced the peak current by providing a porous, high-surface-area network, while the addition of SDS enabled remarkable preconcentration via electrostatic interactions and conferred antifouling properties. The oxidation of LC was an irreversible, predominantly diffusion-controlled process with a one-electron, one-proton rate-determining step. Under optimized conditions, the sensor exhibited a wide linear dynamic range (4.0 nM–22 μM in buffer) with a limit of detection of 0.9 nM in artificial tear fluid, and was successfully applied to a commercial nasal spray, with recoveries of 99.15–100.80% (RSD ≤ 1.12%). As a result, we were able to detect LC either alone or in the presence of azelastine HCl (AZE) or emedastine difumarate (EMD) using square wave voltammetry. The AGREE metric gave a score of 0.79, indicating the greenness of the overall analytical procedure. The sensor is suitable for routine quality control and ocular pharmacokinetic studies.

Keywords: carbon nanotubes; cesium chloride; electrochemical sensor; green analytical chemistry; levocabastine; tear samples

Check for updates

Received: 27 September 2026
Revised: 16 October 2026
Accepted: 18 October 2026
Published: 30 October 2026

Copyright: © 2026 by the authors. Licensee MDPI, Basel, Switzerland. This article is an open access article distributed under the terms and conditions of the Creative Commons Attribution (CC BY) license.

1. Introduction

Antihistamines are one of the most commonly prescribed types of drugs for treating allergies, such as seasonal and recurrent allergic rhinitis, urticaria, allergic conjunctivitis, and reactions to insect bites or stings. Several antihistamines are also used to stop motion sickness, and they are sometimes given to help with nausea and vomiting that happen after

surgery or chemotherapy [1]. These agents primarily function by competitively inhibiting histamine at H1 receptors, thereby reducing histamine-induced vasodilation, heightened vascular permeability, pruritus, and mucus hypersecretion, ultimately mitigating clinical manifestations such as itching, swelling, and excessive nasal and ocular discharge [2]. Levocabastine (LC), marketed as Livostin, is a second-generation, highly selective histamine H1 receptor antagonist, mainly used topically to treat allergic conjunctivitis. It is commonly marketed as a nasal spray and eye drops for the management of seasonal allergic rhinitis and itchy eyes, respectively [3,4]. The drug demonstrates a fast onset and several hours of antihistaminic activity after its local administration. Beyond its classical H1-antagonist properties, LC has been reported as a potent and highly selective antagonist of the neurotensin receptor subtype NTS2, with undetectable activity at other neurotensin receptor subtypes [5]. LC's distinctive receptor selectivity has therefore made this compound one of the most widely used pharmacological tools to interrogate neurotensin receptor function not only in the central nervous system but also in peripheral tissues. In experimental investigations, LC has been found to decrease locomotor activity; this effect was, however, less pronounced compared to other antihistamines such as diphenhydramine, ketotifen, and azelastine [6], consistent with its second-generation nature and poor central nervous system penetration. Multiple randomized clinical trials have also established that LC nasal spray is significantly more effective than placebo in decreasing the frequency and amplitude of nasal symptoms in patients with seasonal allergic rhinitis and has demonstrated a good safety and tolerability profile [7]. Considering its therapeutic relevance, distinct receptor selectivity, and growing clinical applications, there still remains a need for the development of sensitive methods for the assay of LC in pharmaceutical formulations, such as nasal sprays and eye drops, and in tear fluid for quality control and ocular pharmacokinetic studies [8]. Few studies have addressed the analytical determination of LC and its related substances, e.g., one stability-indicating RP-HPLC method for its assay in bulk drug and ophthalmic suspensions [9], and two LC-MS/MS techniques for its detection in blood along with other antihistamine drugs [10,11]. Chromatographic techniques, although robust and reliable, present important disadvantages for routine analysis, such as high cost, the need for highly skilled analysts, extensive sample preparation, and considerable volumes of organic solvents. In contrast, electrochemical methods are sensitive, selective, inexpensive, and simple to use, require minimal sample preparation and small sample volumes, and can be miniaturized for portable detection [12,13]. To our knowledge, no electroanalytical method has been described for the determination of the LC drug, which necessitates the construction of a straightforward, sensitive, and reliable sensing platform. Pristine (unmodified) electrodes, including bare carbon paste electrodes, although inexpensive, often suffer from limited sensitivity [12], sluggish electron transfer kinetics, high oxidation overpotentials, and surface fouling caused by the adsorption of oxidation products, which results in poor reproducibility and restricts their use for the determination of drugs at trace levels. Modifying the electrode surface with nanomaterials is therefore a widely adopted strategy to overcome these limitations by increasing the electroactive surface area, accelerating electron transfer, and improving the selectivity and stability of the response.

Multi-walled carbon nanotubes (MWCNTs) are considered one of the most widely used electrode-modifying nanomaterials when developing an electroanalytical method [14–17]. This is attributed to their unique structural and electrical properties [18,19]. These carbon nanotubes are typically characterized as cylindrical allotropes of graphene composed of sp^2-hybridized carbon atoms, demonstrating outstanding electrical conductivity, significant effective surface area, and advantageous interfacial properties for electron transfer processes. Their chirality and diameter significantly influence their physicochemical properties, resulting in great mechanical strength, increased thermal conductivity, improved charge carrier

mobility, and heightened chemical reactivity [20]. As a result, MWCNT-based materials have been extensively used in transistors, solar energy devices, and particularly in electrochemical sensors. They have also been identified as effective catalyst supports in fuel cells to enhance electrocatalytic performance [21,22], and they have been successfully utilized to increase sensitivity in pharmaceutical analysis [23,24], serve as protective coatings in corrosion science [25], and support drug delivery and drug design applications [26,27].

Cesium (Cs) is a soft alkali metal with a low ionization energy, which readily loses its valence electron to form the Cs^+ cation; therefore, in nature, it occurs only in ionic compounds, such as cesium chloride (CsCl) and cesium nitrate ($CsNO_3$) [28]. CsCl has a simple cubic crystal structure, with Cs^+ (174 pm) and Cl^- (181 pm) ions of similar ionic radii [29]. In this work, CsCl was used as an ionic salt, so the modifier consists of Cs^+ cations with Cl^- counter ions, and not of metallic cesium or cesium nanoparticles. Regarding electrochemical analytical methods, CsCl was previously used as a modifier in the drug determination system by our research group [30,31]. In the same context, sodium dodecyl sulfate (SDS), an anionic surfactant, has numerous applications in the electrochemical field [32]. Nevertheless, MWCNTs and CsCl each have limitations when used alone. MWCNTs tend to aggregate into bundles because of strong van der Waals and π–π interactions, which reduces the accessible surface area and the number of active sites, while CsCl is an ionic crystalline salt that does not provide an electronically conductive network and forms isolated crystals when dispersed in the carbon paste. Combining the two materials was therefore proposed so that CsCl is dispersed over the MWCNT walls, which may reduce their aggregation and create a porous, highly conductive, high-surface-area architecture that facilitates ion transport and electron transfer. This rationale is supported by the voltammetric results, as CsCl or MWCNTs alone produced only a marginal improvement in the oxidation signal of LC, whereas their combination increased the peak current about five-fold (Figure 1, Section 3.1). Even with the MWCNTs/CsCl composite, the electrode surface remains susceptible to fouling by the adsorption of drug oxidation products, and the response at trace levels may be limited by the weak accumulation of the analyte at the electrode/solution interface. Anionic surfactants such as SDS can address both problems, as they form a thin film on the electrode surface that attracts positively charged groups of the analyte electrostatically (preconcentration), facilitates electron transfer, and reduces the non-specific adsorption of oxidation products [32]. At pH 7.0, LC exists in a zwitterionic form bearing a protonated amine group, which is attracted to the negatively charged sulfate head groups of SDS. Therefore, SDS was applied as a thin film over the composite to enhance the sensitivity and resistance to fouling of the sensor. This was confirmed by the further increase in the peak current from 69 to 89 μA, accompanied by a cathodic shift in the peak potential (Section 3.1).

In this study, we developed a novel carbon paste electrode (CPE) modified with MWCNTs, CsCl, and SDS and applied it for LC detection in bulk solution, artificial tears, and nasal spray pharmaceutical formulations. The novelty of this work can be summarized as follows: (i) it presents, to the best of our knowledge, the first electroanalytical method for the determination of LC, filling a gap in the literature where only chromatographic methods are available; (ii) the unique sensor design, in which the MWCNTs/CsCl composite provides a porous, high-surface-area conductive network, while the anionic SDS film preconcentrates the analyte electrostatically and imparts antifouling properties, increases the peak current more than six-fold compared with the bare electrode; (iii) it enables the determination of LC in artificial tear fluid at the nanomolar level (LOD = 0.9 nM), which supports its potential use in ocular pharmacokinetic studies; and (iv) it allows the selective determination of LC in the presence of the co-administered antihistamines AZE and EMD, with a greenness profile supported by the AGREE metric.

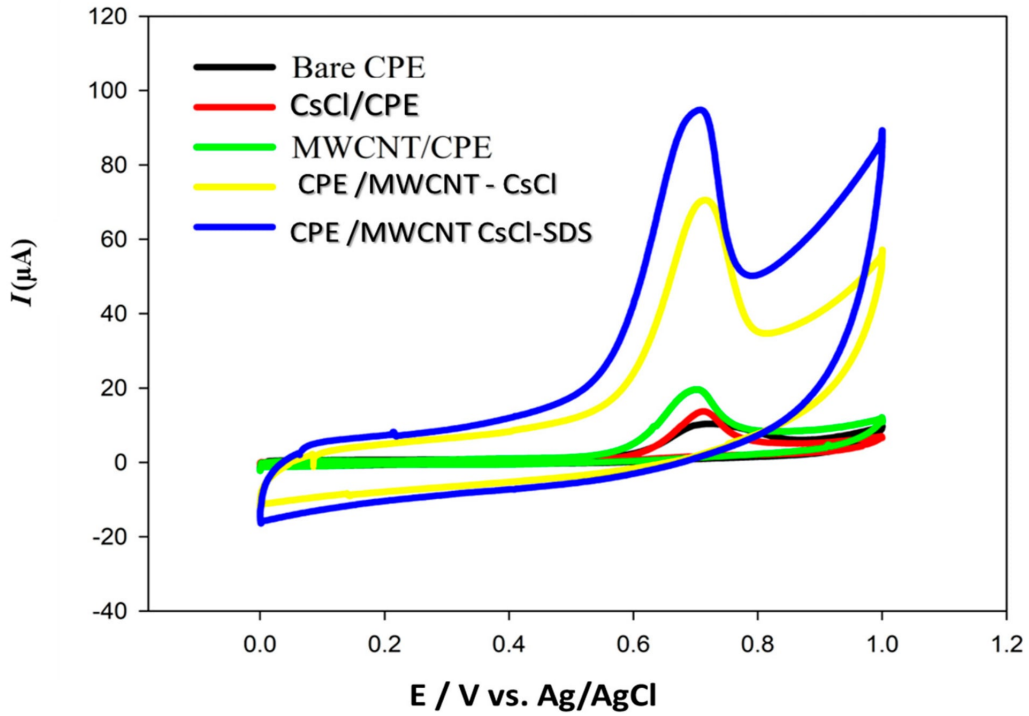


Figure 1. Effectof different modifiers on the oxidation of LC of 1.0×10^{-4} in B-R buffer (pH 7.0) at the bare CPE, CsCl/CPE, MWCNT/CPE, CPE /MWCNT-CsCl, and CPE /MWCNT CsCl-SDS at scan rate 100 mV s^{-1}.

2. Materials and Methods

2.1. Chemicals and Reagents

A pure reference standard of levocabastine (LC) was obtained from Janssen Pharmaceutical N.V. (Beerse, Belgium), with its purity checked using the reported [9] and pharmacopeial [33] methods and found to be 100.02% ± 0.90% and 99.98% ± 0.87%, respectively. Azelastine hydrochloride (AZE) was provided by European Egyptian Pharm Co. (Cairo, Egypt), and emedastine difumarate (EMD) was supplied by Chem Swiss, SIGMA Co. (Cairo, Egypt). Commercial LIVOSTIN® N.S. nasal spray (labeled to contain 0.5 mg LC/mL, Janssen Cilag) was supplied by Dawaya (Cairo, Egypt). Multi-walled carbon nanotubes (MWCNTs) were purchased from NanoLab Inc. (Waltham, MA, USA; Cat. No. PD15L520; purity > 95%; supplier-specified outer diameter of 15 ± 5 nm, length of 5–20 µm, and specific surface area of 200–400 m^2/g). TEM examination of the prepared nanocomposite showed the MWCNTs as elongated, hollow cylindrical structures with observed diameters ranging from 40 to 80 nm, as described in Section 3.2.1. Synthetic graphite powder (particle size <20 µm; CAS No. 7782-42-5) was purchased from Sigma–Aldrich (Steinheim, Germany; Cat. No. 282863). Commercial artificial tear formulation (Solofresh® ophthalmic solution; Orchidia Pharmaceutical Industries, Cairo, Egypt) was purchased from the local pharmaceutical market in Egypt. According to the product label, each mL contains 0.2% *w*/*v* sodium hyaluronate as the active lubricating component, together with sodium chloride, potassium chloride, boric acid, and sodium borate in purified water, with a labeled pH of 7.2 ± 0.2. Sodium dodecyl sulfate (SDS, purity ≥ 99.0%), paraffin oil, and Nafion binder (5 wt% dispersion in lower aliphatic alcohols and water) were procured from Sigma–Aldrich (Steinheim, Germany). Cesium chloride (CsCl) was obtained from GRG (West Bromwich, UK) and used as received without further purification. Concentrated nitric acid (HNO_3, 68%), diethyl ether, sodium hydroxide, phosphoric acid, boric acid, and acetic acid were purchased from El-Nasr Pharmaceutical Chemicals Co. (ADWIC,

Cairo, Egypt) and Sigma–Aldrich (Steinheim, Germany). Britton–Robinson (B–R) buffer solutions were prepared by mixing equal volumes of phosphoric, boric, and acetic acids (0.04 M each), with the pH adjusted using 0.20 M sodium hydroxide. All chemicals were of analytical grade and used as received, and deionized water was used in all experimental procedures.

2.2. Apparatus

Voltammetric analysis was conducted using a Bio-Logic SP-150 potentiostat (Bio-Logic Science Instruments, Seyssinet-Pariset, France) with a single-compartment three-electrode cell. The working electrode was an in-house laboratory-fabricated carbon paste electrode, as described in Section 2.3. The auxiliary electrode was a platinum wire (CH Instruments, Austin, TX, USA, Cat. No. CHI115), and the reference potentials were measured relative to an Ag/AgCl (3.0 M NaCl) reference electrode (CH Instruments, Austin, TX, USA, Cat. No. CHI111). Scanning electron microscopy (SEM) analysis was performed using a Quanta FEG 250 scanning electron microscope (Thermo Fisher Scientific (FEI), Hillsboro, OR, USA). High-resolution transmission electron microscopy (HR-TEM) analysis was performed using a JEM-2100 HRTEM microscope (JEOL Ltd., Tokyo, Japan) operated at an accelerating voltage of 200 kV with a point-to-point resolution of 0.2 nm. X-ray diffraction (XRD) patterns were recorded using a PANalytical X'Pert PRO diffractometer (Malvern Panalytical, Almelo, The Netherlands) operated with Cu Kα radiation ($\lambda = 0.15406$ nm) over a 2θ range of 10–80°. The average crystallite size (D) was calculated using the Debye–Scherre equation $D = (K\lambda)/(\beta \cos\theta)$, where K is the shape factor (0.9), λ is the X-ray wavelength (0.15406 nm), β is the full width at half maximum (FWHM) in radians (corrected for instrumental broadening), and θ is the Bragg angle. Fourier transform infrared (FTIR) spectra were recorded on an Agilent Cary 630 FTIR spectrophotometer (Agilent Technologies, Santa Clara, CA, USA). Solution pH was measured using a Cyberscan 500 digital pH meter (Eutech Instruments, Singapore, Singapore) equipped with an Eutech combination glass electrode. All tests were conducted at a controlled room temperature of 25 °C for consistency and reliability.

2.3. Fabrication of the Sensors

Several sensors were fabricated and tested. To fabricate a bare carbon paste electrode (CPE), 0.50 g of graphite powder was accurately combined with 0.30 mL of paraffin oil in a glass mortar until a homogeneous paste was achieved. The paste was firmly packed into the electrode cavity, and the surface was polished using smooth filter paper to obtain a uniform, smooth surface. For the modification processes, 0.025 g of MWCNTs was first refluxed in concentrated HNO_3 for 4.0 h and subsequently washed with deionized water until a neutral pH was reached, then dried to obtain functionalized MWCNTs (F-MWCNTs). To fabricate the CPE/MWCNT and CPE/ CsCl sensors, 0.025 g of these previously functionalized MWCNTs or CsCl was combined with 0.50 g of graphite powder and 0.30 mL of paraffin oil. For the synthesis of the MWCNT/CsCl nanocomposite, 10.0 mg of F-MWCNTs and 60.0 mg of CsCl were dispersed in 5.0 mL of ethanol containing 50 µL of 5 wt% Nafion solution as a binder. The suspension was sonicated in an ultrasonic bath (37–40 kHz, 100–120 W) for 30 min at 25 ± 2 °C to disrupt F-MWCNT agglomerates and ensure the homogeneous dispersion of F-MWCNTs and CsCl in the presence of Nafion. Subsequently, the suspension was magnetically stirred during solvent evaporation to maintain dispersion homogeneity and prevent particle sedimentation, phase separation, and re-agglomeration, thereby promoting the formation of a uniform and completely dried MWCNT/CsCl composite powder. The prepared MWCNT/CsCl composite was subsequently blended with graphite powder in a weight ratio of 5% composite to 95% graphite. The solid mixture was dispersed in

diethyl ether and stirred magnetically until the solvent evaporated. Subsequently, paraffin oil was incorporated into the dry mixture to form the paste. The paste was then inserted into the electrode body. Finally, to fabricate the final CPE/MWCNT-CsCl/SDS sensor, the surface was modified by applying 10 µL of a 1.0×10^{-3} M sodium dodecyl sulfate (SDS) aqueous solution and allowing it to dry at ambient temperature for 10 min.

2.4. Electrochemical Behavior of LC Using Cyclic Voltammetry (CV) and Calibration Curve Construction

A stock standard solution of LC (1.00×10^{-3} M) was prepared by accurately weighing 4.25 mg of pure LC, dissolving it in B–R buffer (pH 7.0), and adjusting the volume to 10.0 mL in a volumetric flask (0.425 mg/mL). The prepared stock solution was stored at 4 °C in the dark and freshly diluted prior to analysis. Working solutions were prepared by appropriate dilution of the stock solution with B–R buffer (pH 7.0). All measurements were carried out in a single-compartment cell containing 5.0 mL of solution at 25 °C, with the potential scanned in the positive direction. For the blank, 5.0 mL of B-R buffer (pH 7.0) was transferred into the electrolytic cell. The auxiliary, reference, and working electrodes were immersed in the solution, and the electrochemical signals were recorded using CV. To evaluate the electrochemical behavior, 0.50 mL of the LC stock solution (1.00×10^{-3} M) was transferred to a 5.0 mL volumetric flask and diluted to the mark with B–R buffer (pH 7.0), giving a final LC concentration of 1.00×10^{-4} M. The obtained solution was placed in the electrochemical cell for analysis, and cyclic voltammograms were recorded from 0.0 to +1.0 V. The scan rate was varied from 10 to 100 mV s^{-1} in the scan rate study (Section 3.3.2), and 100 mV s^{-1} was selected for the remaining CV experiments. For the calibration curves, serial dilutions were prepared from the stock solution and measured by SWV. SWV was recorded from +0.40 to +1.10 V with a frequency of 20 Hz, a pulse amplitude of 25 mV, and a step potential of 0.5 mV, corresponding to an effective scan rate of 10 mV s^{-1}. Cyclic voltammograms were recorded from 0.0 to +1.0 V at scan rates of 20–100 mV s^{-1}. All measurements were carried out in 5.0 mL of solution at 25 °C.

2.5. Application of CPE/MWCNT/ CsCl/SDS for Determination of LC in Artificial Tear Fluid (ATF)

One mL of artificial tear fluid (ATF) was spiked with LC and diluted to a total volume of 10 mL, achieving a final concentration of 1.0×10^{-5} M of the tested drug. Then, aliquots equivalent to (5.0×10^{-9}–2.0×10^{-6} M) of LC were added to 5 mL of B-R buffer of pH 7 of LC were added to 5 mL of B-R buffer at pH of 7.

2.6. Application of CPE/MWCNT- CsCl/SDS for Determination of LC in Pharmaceutical Preparation

The contents of two bottles of LIVOSTIN® N.S. nasal spray were mixed, and aliquots equivalent to 4.25 mg of LC (8.5 mL) were transferred to a 10 mL volumetric flask, then diluted with B–R buffer (pH 7.0) to obtain a stock solution of 1.0×10^{-3} M LC (equivalent to 0.425 mg/mL). The resulting solution was filtered through a 0.45 µm membrane filter prior to analysis. The pharmaceutical content was determined using SWV and the regression equation. To confirm the accuracy and exclude matrix interference from formulation excipients, the standard addition technique was carried out by spiking the formulation sample with three known concentration levels of pure LC standard (0.50, 1.00, and 1.50 µM), and the corresponding recovery percentages (Recovery%) and relative standard deviations (RSD%) were calculated.

3. Results and Discussion

3.1. Effect of Different Modifiers on the Voltammetric Response of LC

Figure 1 depicts how different modifiers influence the oxidation behavior of LC in B-R buffer (pH 7). The assessed electrodes were bare CPE, CPE/CsCl, CPE/MWCNT, CPE/MWCNT-CsCl, and CPE/MWCNT-CsCl/SDS. At the bare CPE, LC exhibited a weak oxidation peak current of 10.0 µA. Adding CsCl alone resulted in a slight increase to 14.0 µA, whereas MWCNTs alone doubled the oxidation signal to 20.0 µA compared with the bare electrode. This behavior can be attributed to the aggregation of MWCNTs when used alone, which limits the available active surface, as well as the crystalline, non-conductive nature of CsCl, which appears as isolated cubic crystals on the graphite matrix (Figure 2B). In contrast, combining CsCl and MWCNTs markedly increased the peak current from 10.0 µA to 69.0 µA. This enhancement is attributed to the ability of CsCl to disperse and form spherical microstructures on MWCNTs. Naturally conductive MWCNTs facilitate electronic interactions with CsCl, resulting in a porous surface that promotes ion transport between the electrode surface and the electroactive species, thereby offering a large effective surface area favorable for electrochemical reactions. The comparison is based on peak currents recorded in a single set of measurements under identical conditions, and no statistical test was applied. The proposed fabrication of the CPE/MWCNT-CsCl/SDS sensor and the electrochemical oxidation mechanism of LC are illustrated in Scheme 1 and discussed in Section 3.3.3. The anodic peak current further increased to 94.4 µA after modification with the anionic SDS film (representing an additional increase of ~37%), with no appreciable change in the peak potential. This further signal amplification is assigned to the electrostatic accumulation of LC at the interface through its protonated amine group, rather than to a change in electron transfer kinetics. The presence of LC in zwitterionic form at pH 7 does not interfere with the electrode reaction, as the anionic SDS film facilitates drug accumulation at the interface by attracting the protonated amine group, thereby increasing the surface concentration of LC and hence the peak current. The SDS film is also expected to reduce non-specific adsorption of oxidation products. Although SDS is applied as a simple drop-cast film (10 µL, dried for 10 min), its use is particularly advantageous for complex matrices such as tear fluid, where fouling by matrix components and reaction product adsorption is a major concern for signal reproducibility.

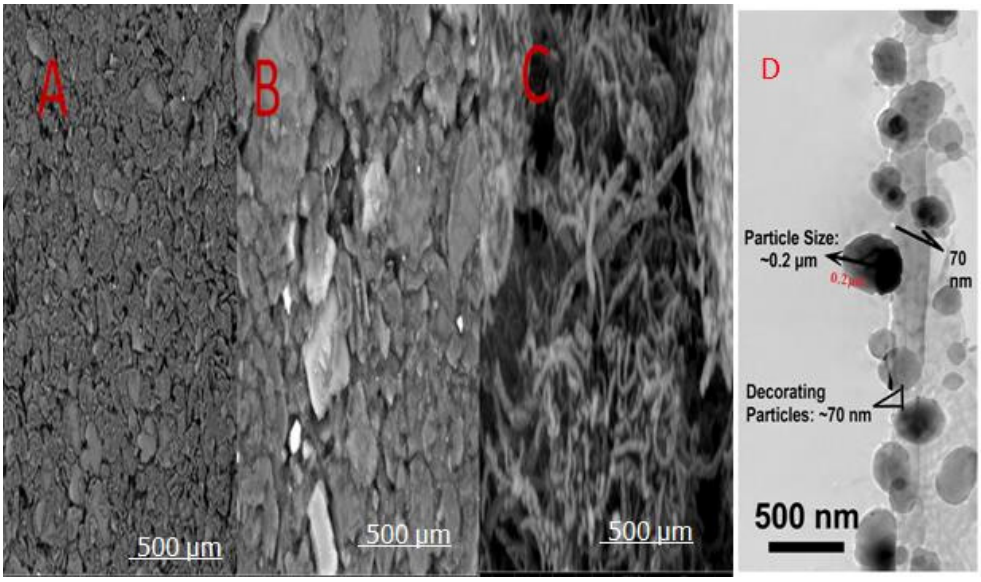
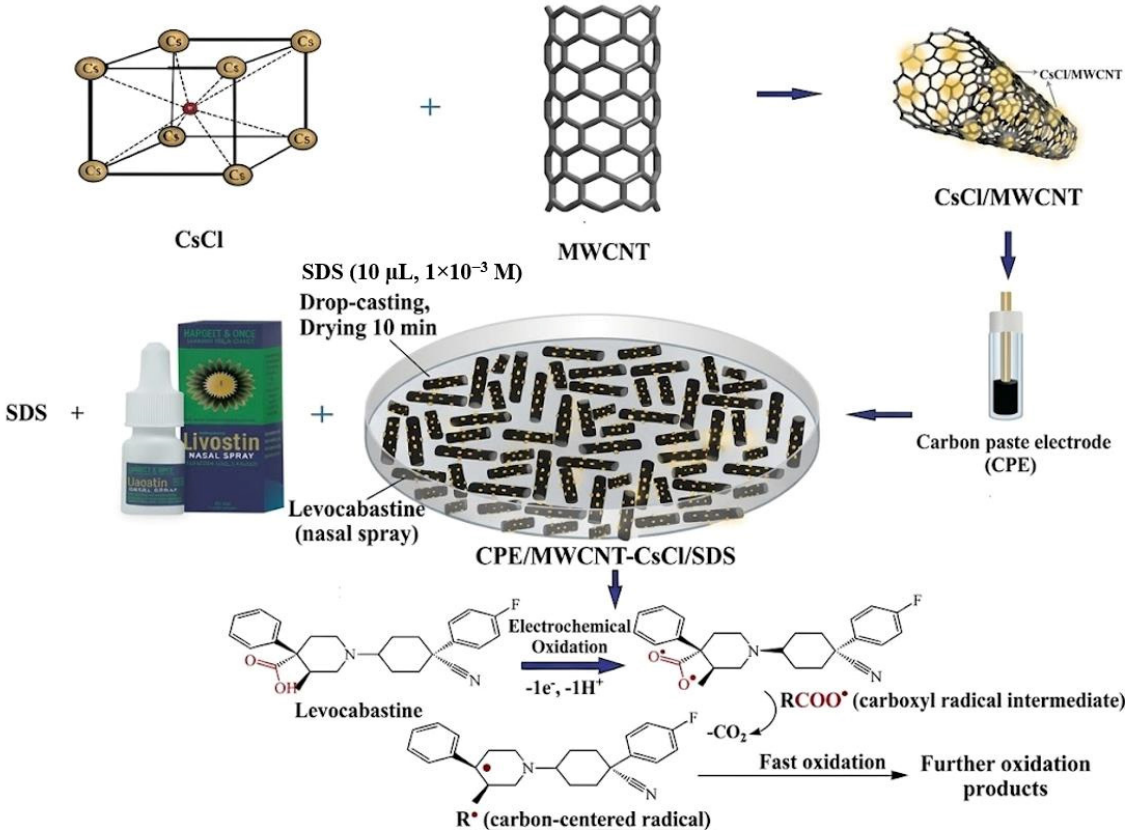


Figure 2. SEM images of (**A**) bare CPE, (**B**) CPE/CsCl, (**C**) CPE/MWCNT, and (**D**) TEM of MWCNT-CsCl composite.



Scheme 1. Schematic representation of the preparation of the CPE/MWCNT–CsCl/SDS sensor, including the SDS surface modification step, and the proposed electrochemical oxidation mechanism of LC.

3.2. Characterization of the Modifier and the Electrode Surface

3.2.1. Characterization of the Modifier (MWCNT-CsCl Composite)

The nanomaterials used for the modification were characterized first by TEM for morphology (Figure 2D), FTIR for functional groups (Figure 3), and XRD for crystalline structure (Figure 4), followed by the characterization of the electrode surface in Section 3.2.2. Since SDS was introduced only as a final surface modification of the fabricated electrode and is not a component of the MWCNT–CsCl composite, the TEM, FTIR, and XRD analyses were primarily performed on the MWCNT–CsCl composite to characterize the structure and properties of the bulk modifier. The contribution of SDS to the sensing interface was evaluated electrochemically in Section 3.1

TEM. We employed transmission electron microscopy (TEM) to examine the interactions among the components of the composite (Figure 2D). The MWCNTs appeared as elongated, hollow cylindrical structures with observed diameters ranging from 40 to 80 nm. CsCl-associated particulate features were observed in the vicinity of the MWCNT structures, suggesting an association of the CsCl phase with the carbon nanostructure.

FTIR. FTIR spectra in the range 4000–500 cm^{-1} were examined to study the nature of the chemical bonds formed. After functionalization of MWCNT with HNO_3, MWCNT-COOH was formed, so IR spectra of pure MWCNT and functionalized MWCNTs (F-MWCNT) were obtained and are shown in Figure 3a. Characteristic bands for aromatic C–H at 3050 cm^{-1} and C–H at 1350 cm^{-1} appeared for pure MWCNT [34], while characteristic bands at 1650 cm^{-1}, 2200 cm^{-1}, and 1250 cm^{-1} corresponding to C=O, O-H bending, and C-O bonds, respectively, were attributed to the formation of COOH groups at the ends of F-MWCNT. The aromatic C=C bond was detected at 1440 cm^{-1} in the spectra

of both pure and F-MWCNT [35]. The peak at 3400 cm^{-1} for F-MWCNT corresponds to the stretching of the OH group of H_2O or the COOH group. FT-IR spectra of CsCl before and after mixing with water (F-CsCl) are also shown in Figure 3b. It is clear that pure CsCl does not give any characteristic bands. As CsCl is mixed with water, CsOH is formed [36], and broad O-H stretching bands at 2100 and 3400 cm^{-1} indicate the presence of free OH^- groups and therefore the presence of free Cs ions that give a characteristic peak at 1630 cm^{-1}. The FT-IR spectrum of the composite synthesized through the combination of CsCl and F-MWCNTs with Nafion is depicted in Figure 3c. The presence of Nafion within the composite can be confirmed by the distinct peak at 1070 cm^{-1}, attributable to the C-F stretching vibrations of the polymer chains. The O-H stretching peaks of the cesium ions experienced a bathochromic shift, indicating an enhancement in hydrogen bonding. The FTIR data provide evidence for both chemisorption and specific interactions between cesium ions and F-MWCNTs. The oxygen-containing functional groups present in F-MWCNTs serve as adsorption sites for Cs^+ ions. The interaction of cesium species with the functionalized MWCNT surface is primarily attributed to electrostatic attraction between Cs^+ ions and these surface groups, with possible contributions from cation–π interactions and surface complexation. Furthermore, the formation of direct chemical bonds is evidenced by the appearance of a band at 781 cm^{-1}, corresponding to the stretching vibration mode of MWCNT-O-Cs, and a band at 1360 cm^{-1}, attributed to the Cs-O bending mode. Such spectral bands indicate effective incorporation of CsCl and its bonding with the MWCNT network.

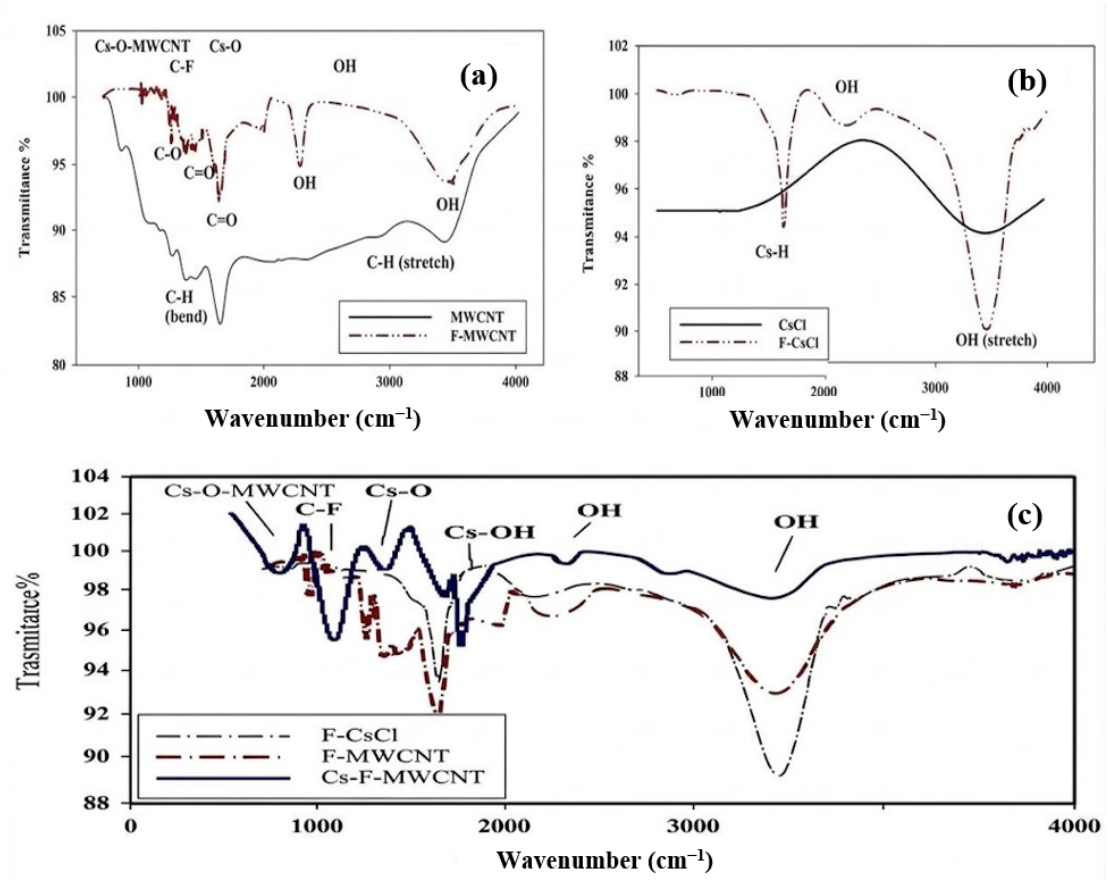


Figure 3. FTIR charts of (**a**) MWCNT and F-MWCNT, (**b**) CsCl and F-CsCl, and (**c**) a comparison between F-CsCl, F-MWCNT, and CsCl/F-MWCNT.

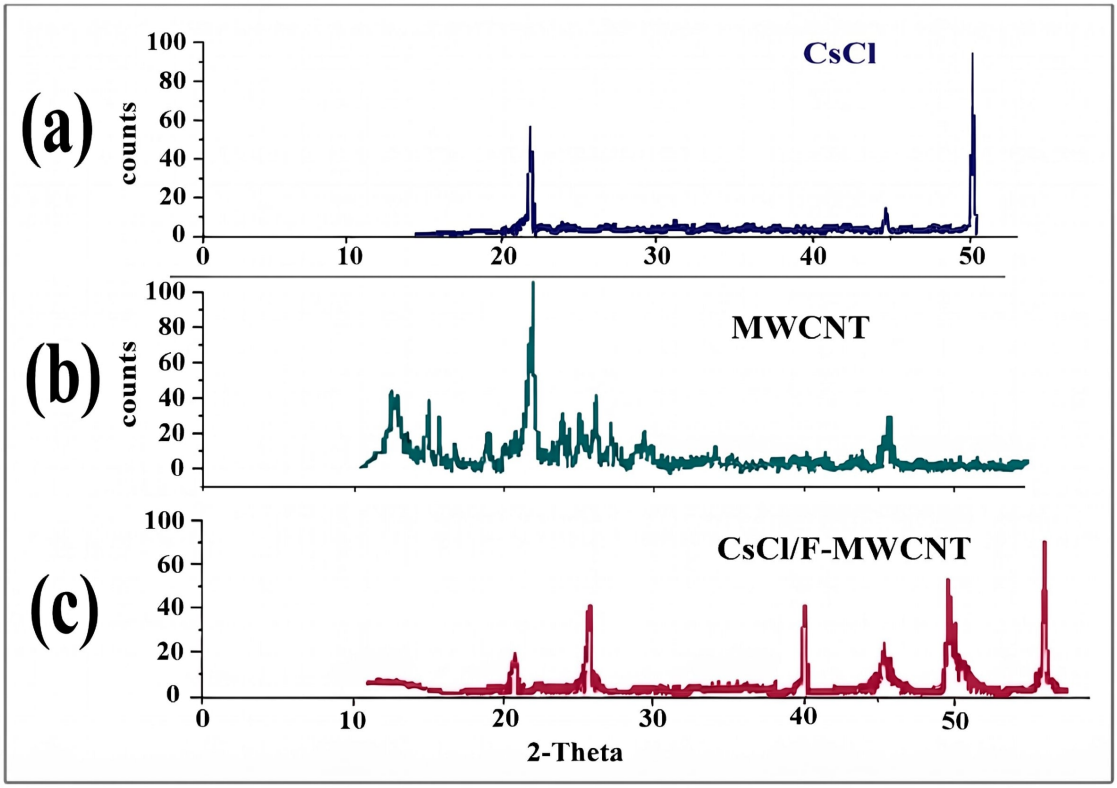


Figure 4. XRD images of (**a**) CsCl, (**b**) MWCNTs, and (**c**) CsCl/F-MWCNT.

XRD Analysis. The crystallographic phase structure of the synthesized nanomaterials was evaluated via XRD (Figure 4). Figure 4a shows the diffractogram of CsCl with sharp and intense XRD diffraction peaks centered at 2θ ≈ 21.7°, 44.5°, and 50.0°, indicating high phase purity and crystallinity, with a chloride atom in the center of the unit cell and a cesium atom at each corner of the cube of the unit cell [37]. In order to determine the crystalline nature of the nanotubes, the XRD pattern of MWCNTs was evaluated (Figure 4b), displaying a main diffraction reflection at 2θ ≈ 22.0° corresponding to the d (002) plane due to an increase in the sp2 C=C layer spacing, which is evidence of the presence of hexagonal graphitized MWCNTs [38]. The other characteristic reflection is located at 2θ ≈ 45.0°, related to the (100) plane of graphite. It is worth noting that the XRD pattern of F-MWCNTs is similar to that of pure MWCNTs, indicating that they still have the same cylinder wall structure as unmodified MWCNTs. After mixing CsCl with F-MWCNTs (Figure 4c), the (002) peak intensity is enhanced, which indicates the shortening of MWCNTs in the sample. This indicates improved purity and crystallinity of the carbon nanotubes. CsCl salt can be easily positioned in the interlamellar space of MWCNTs because of the high atomic X-ray scattering factors of the Cs^+ (54) and Cl^- (18) ions. Thus, Cs^+ was incorporated into the MWCNTs' holes and interacted with oxygen atoms, forming electrostatic bonds and hydrogen bonds with the OH groups, giving diffraction peaks that appear at 2θ ≈ 42°, 44°, and 55°, indexed to (100), (101), and (004) reflections. In summary, CsCl is well chemisorbed into the crystal structure of MWCNTs. Furthermore, the average crystallite size (D) was calculated using the Debye–Scherrer equation:

$$D = \frac{K\lambda}{\beta \cos \theta}$$

where K is the shape factor (0.9), λ is the X-ray wavelength (0.15406 nm for Cu Kα radiation), β is the full width at half maximum (FWHM) in radians, and θ is the Bragg angle. Based on the characteristic (002) peak at 2θ = 22.0°, the average crystallite size of the MWCNTs was calculated to be approximately 12.5 nm, whereas the sharp diffraction peaks of CsCl

yielded a crystallite size of approximately 38.2 nm, confirming the nanoscale features and high phase purity of the modified components. The detailed XRD peak parameters (2θ, (hkl) planes, FWHM, and calculated crystallite sizes) are summarized in Table 1.

Table 1. XRD diffraction parameters and calculated average crystallite size (D) using the Debye–Scherrer equation.

Sample	2θ (°)	(hkl) Plane	FWHM (°)	D Calculated (nm) *
MWCNTs	22.0	(002)	0.64	12.5
F-MWCNTs	22.1	(002)	0.66	12.1
CsCl	21.7	(110)	0.21	38.2
CsCl/F-MWCNT Composite	22.0/21.7	(002)/(110)	0.65/0.22	12.3/36.5

* K = 0.9 (shape factor), λ = 0.15406 nm, β represents the full width at half maximum (FWHM) of the diffraction peak in radians after instrumental broadening correction, θ is the Bragg angle, and D is the average crystallite size calculated using Scherrer's equation.

3.2.2. SEM Characterization of the Electrode Surfaces

The surface morphology of the fabricated electrodes was examined using scanning electron microscopy (SEM) (Figure 2A–C). The bare CPE (Figure 2A) exhibited a relatively smooth, featureless surface, consistent with the typical appearance of carbon paste. Conversely, the CPE/CsCl surface (Figure 2B) exhibited well-defined, glossy cubic crystals of CsCl distributed across the graphite matrix. The CPE/MWCNT electrode (Figure 2C) exhibited a more textured surface characterized by layers of amorphous-like tubular structures that were dispersed throughout.

3.3. Parameter Optimization

3.3.1. Effect of Changing pH of the B-R Buffer

The B-R buffer was utilized to investigate the impact of solution pH on the electrochemical oxidation of LC across a pH range of 2.0 to 10.0 (Figure 5a). As illustrated in the bar chart (Figure 5b), the anodic peak current recorded at the modified CPE/MWCNT-CsCl/SDS electrode was consistently greater than that observed at the bare CPE, regardless of the pH. The peak current increased from 18.54 µA at pH 2.0 to a maximum of 94.38 µA at pH 7.0 and decreased at higher pH values. pH 7.0 gave the highest response among the pH values studied and is close to the physiological pH of tear fluid (≈7.4) and that of the artificial tear formulation used (labeled pH 7.2 ± 0.2), and it was therefore selected for all subsequent measurements. The enhanced response at pH 7.0 may be attributed to the favorable electrochemical environment provided by the MWCNT–CsCl/SDS-modified electrode. The presence of the anionic SDS surface modifier may also contribute to the enhanced response through favorable electrostatic interactions with the protonated form of LC at the electrode interface. Furthermore, we analyzed the evolution of the peak potential (E_p) as a function of pH (Figure 5c). A cathodic linear shift in the peak potential was observed with increasing pH, thereby indicating the involvement of protons in the electrode reaction. The relationship between E_p and pH is expressed by the following linear regression equation: $E_p(V) = -0.0568\ pH + 1.2112$ ($R^2 = 0.9988$). The slope of −56.8 mV pH^{-1} closely approaches the theoretical value of −59.2 mV pH^{-1} at 25 °C, indicating proton participation in the electrode reaction and an approximately equal proton-to-electron stoichiometry.

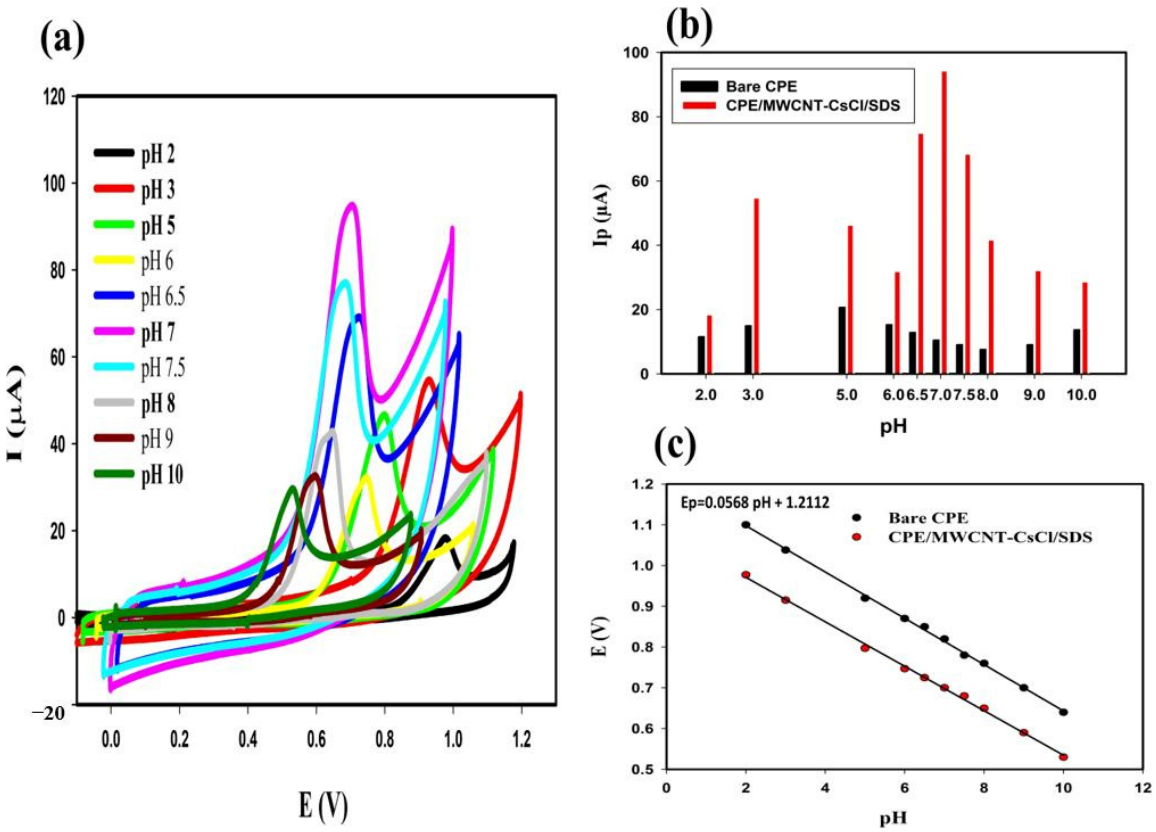


Figure 5. (**a**) Cyclic voltammograms of 1.0×10^{-4} M LC in B-R over varying pH values from 2.0 to 10.0. (**b**) Bar chart of Ip versus pH at bare CPE and CPE/MWCNT-CsCl/SDS. (**c**) Plot of Ep versus pH at bare CPE and CPE/MWCNT-CsCl/SDS.

3.3.2. Effect of Scan Rate

We investigated the electrochemical kinetics of LC at the CPE/MWCNT- CsCl/SDS electrode by obtaining CV of 1.0×10^{-4} M LC at scan rates (ν) ranging from 20 to 100 mV s^{-1} (Figure 6a). The plot of log Ip against log ν (Figure 6b) gave a slope of 0.39, which approximates the theoretical value of 0.5 anticipated for species governed by diffusion [39]. For an irreversible, diffusion-controlled electrode process, the slope of the Ep versus log ν (Figure 6c) is given by 2.303RT/2αnF, corresponding to 0.05916/2αn V $decade^{-1}$ [40]. From this linear relationship, a slope of 0.087 V $decade^{-1}$ was practically obtained, corresponding to an αn value of 0.34. Based on what is reported on the oxidation of drugs containing carboxylic acid groups, the removal of one electron is usually suggested [41,42]. Finally, a scan rate of 100 mV s^{-1} was selected for the subsequent cyclic voltammetric experiments.

3.3.3. Proposed Oxidation Mechanism of LC

According to the above-obtained data, it can be assumed that LC oxidation is an irreversible diffusion-controlled process in which one electron and one proton are involved. The electro-oxidation is related to proton exchange in the buffer solution; one electron is liberated in the oxidation process due to the oxidation of a carboxylic acid group in LC. The oxidation is proposed to proceed through three consecutive steps: (i) preconcentration of LC at the SDS-modified electrode surface, presumably through electrostatic interactions, (ii) a coupled loss of one electron and one proton from the carboxylic group, generating a highly reactive and unstable carboxyl radical (R–COO•), which is proposed to represent the rate-determining electrochemical step; and (iii) rapid irreversible decarboxylation with

release of CO_2 to generate a carbon-centered radical (R•), followed by further fast oxidation to the final oxidation products (Scheme 1).

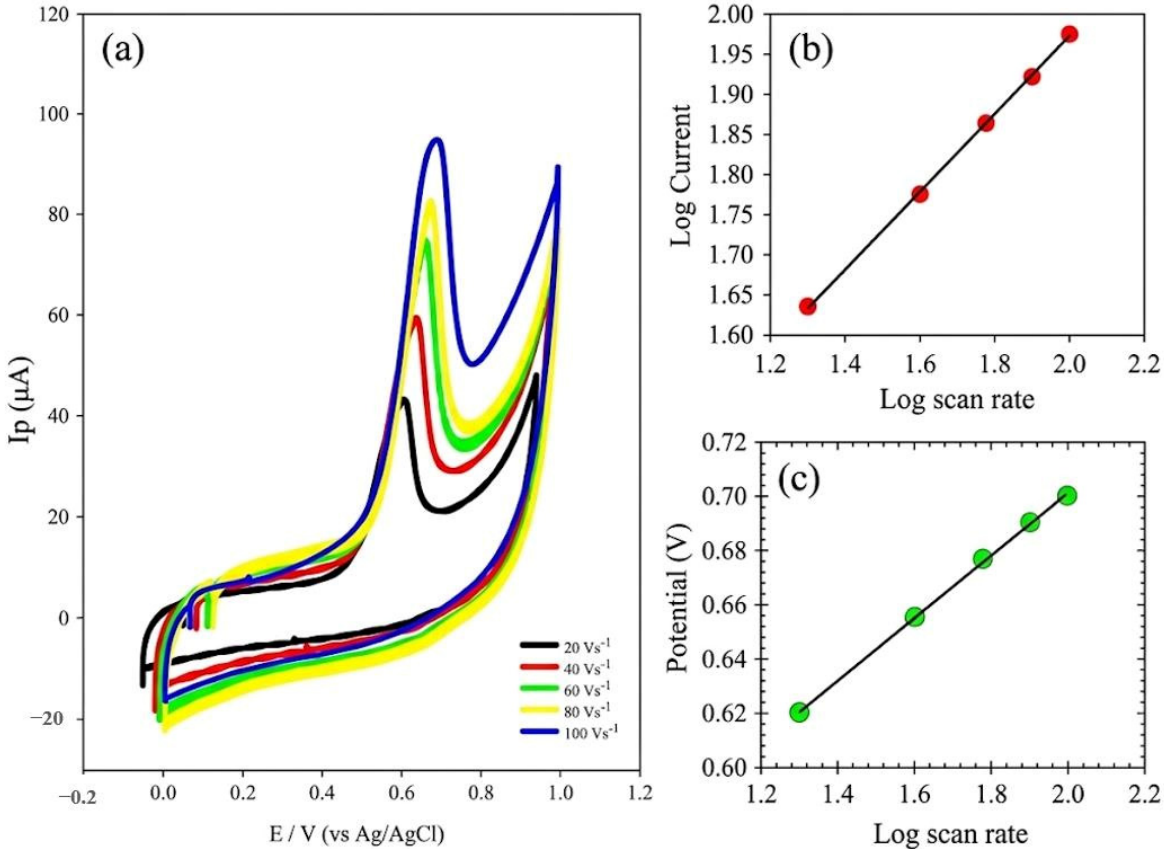


Figure 6. (**a**) Cyclic voltammograms of 1×10^{-4} M LC at varying scan rates (v) from 20 to 100 mV s^{-1}. (**b**) Relation between the log of the anodic peak current and the log of the scan rate. (**c**) Relation between the anodic peak potential and the log of the scan rate.

This proposed pathway is consistent with the reported decarboxylative oxidation behavior of carboxylic acids in Kolbe-type electrochemical processes [41,42]. However, the proposed intermediates and subsequent products were not directly identified in the present study; therefore, the mechanism is proposed on the basis of the observed voltammetric behavior, pH dependence, kinetic analysis, and molecular structure of LC rather than confirmed by direct product analysis.

3.4. Calibration Curve Construction in Buffer

We employed SWV to quantify LC since it is more sensitive and reduces electrostatic charging currents compared with the conventional CV. The electrochemical response of the CPE/MWCNT-CsCl/SDS sensor was evaluated with increasing concentrations of LC in B-R buffer (pH 7.0) under the SWV conditions (Figure 7). Under the optimum conditions, two linear calibration curves were constructed (Figure 7a,b) from 4.0×10^{-9} M to 1.8×10^{-6} M and from 1.8×10^{-6} M to 2.2×10^{-5} M, respectively. We evaluated the analytical performance of the proposed sensor by examining the calibration data.

$$\text{Lower range} = \text{Ip } (\mu\text{A}) = 2.42\ \text{C } (\mu\text{M}) + 1.07\ (R^2 = 0.9992)$$

$$\text{Higher range} = \text{Ip } (\mu\text{A}) = 0.85\ \text{C } (\mu\text{M}) + 3.89\ (R^2 = 0.9985)$$

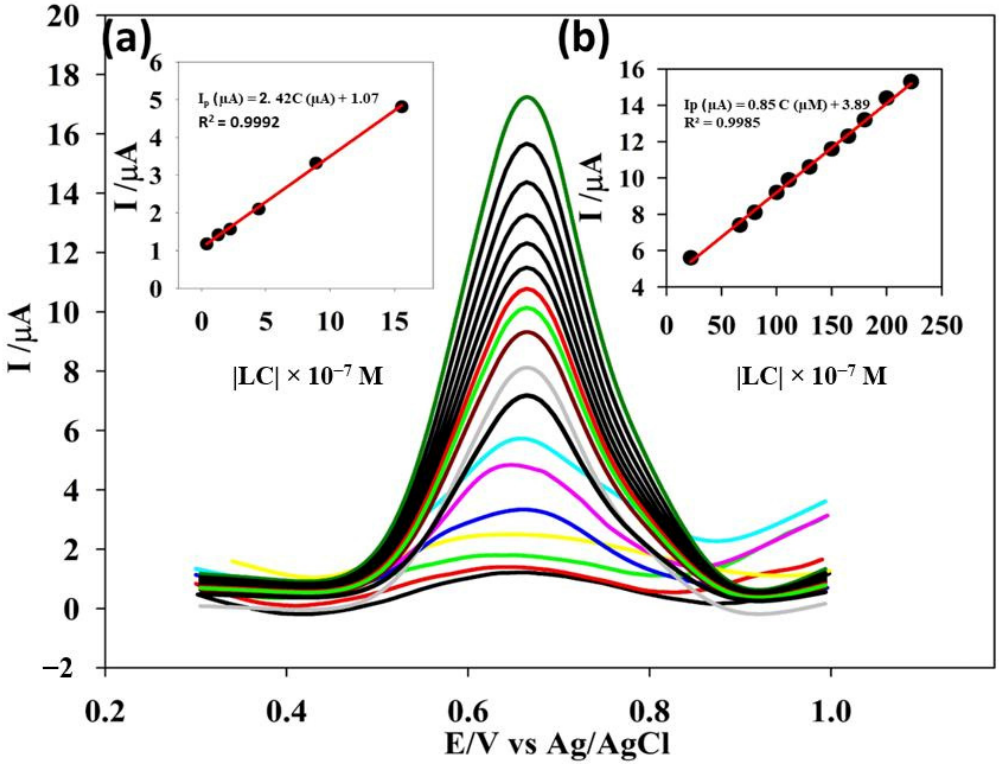


Figure 7. SWV curves of LC at various concentrations in B–R buffer (pH 7.0). Insets (**a**) and (**b**) show the linear calibration plots for 4.0 nM–1.8 μM and 1.8–22 μM, respectively.

The CPE/MWCNT-CsCl/SDS sensor showed excellent linearity, indicating its capability to properly detect LC. The limit of detection (LOD) and limit of quantification (LOQ) were calculated using the formulas 3 σ/S and 10 σ/S, respectively, where σ represents the standard deviation of the intercept, and S denotes the slope of the calibration curve [43]. The established limits of detection (LOD) and quantification (LOQ) were 0.7 nM and 2.3 nM, respectively (Table 2).

Table 2. Analytical performance parameters for the quantification of levocabastine in spiked artificial tear fluid, utilizing the proposed SWV.

Parameters	BR Buffer (Range I)	BR Buffer (Range II)	ATF Sample
Linearity (M)	4.0×10^{-9}–1.8×10^{-6}	1.8×10^{-6}–2.2×10^{-5}	5.0×10^{-9}–2.0×10^{-6}
LOD (M)	7.0×10^{-10}	—	9.0×10^{-10}
LOQ (M)	2.3×10^{-9}	—	3.0×10^{-9}
Slope	2.42	0.85	0.171
SE of slope	0.018	0.021	0.024
Intercept	1.07	3.89	1.22
SE of Intercept	0.035	0.052	0.07
Correlation coefficient (r)	0.9992	0.9985	0.9987
Accuracy (Recovery %, Mean ± SD, n = 5)	99.85 ± 0.82	—	98.36 ± 0.95
Precision (RSD %)	0.82	—	0.96

3.5. Analytical Applications in Real Samples and Statistical Analysis

We first evaluated the efficacy of the proposed approach by quantifying LC levels in artificial tear fluid (ATF). ATF was selected to replicate the location where the medication would be administered in the eye. The validation results presented in Table 2, along with the mean recoveries of 98.36 ± 0.95% (average of the three levels, n = 5 per level), suggest minimal influence from the matrix. The sensor was additionally employed to examine the commercial medicine LIVOSTIN® nasal spray. This formulation is frequently employed for the symptomatic relief of allergic rhinitis caused by environmental allergens. The standard addition method was employed to assess the accuracy of the method. The mean recoveries were 99.15 ± 1.01%, 100.20 ± 0.90%, and 100.80 ± 1.13% at the three spiked levels (RSD 0.90–1.12%, n = 5; Table 3). These data indicate that the evaluation of LC is not influenced by the use of common formulation excipients, such as benzalkonium chloride and disodium edetate. The content of LC found in the nasal spray was 99.60 ± 0.80% of the labeled amount (n = 5), which lies within the acceptance range of 90.0–110.0% specified in the registered manufacturer's specifications for the product. No pharmacopeial monograph for levocabastine nasal spray was available to us. The results are summarized in Table 4. Furthermore, to validate the precision of our proposed sensor, the outcomes from the suggested sensor were statistically compared with those from the approved pharmacopeial approach (Table 5) [33]. It should be noted that the statistical comparison was performed on the pure drug against the official titrimetric method, which is limited to bulk raw materials. For the nasal spray and artificial tear fluid, the standard addition method was used to eliminate matrix effects, as reported HPLC and LC-MS/MS methods either lack sufficient sensitivity for nanomolar tear fluid analysis or require specialized instrumentation.

Table 3. Recovery of LC in LIVOSTIN® nasal spray by the standard addition method (n = 5).

	Added (μM)	Found (μM),	Recovery (%), Mean ± SD	RSD (%)
LIVOSTIN® Nasal Spray	0.50	0.496	99.15 ± 1.01	1.02
	1.00	1.002	100.20 ± 0.90	0.90
	1.50	1.512	100.80 ± 1.13	1.12

Table 4. Content of LC in LIVOSTIN® nasal spray.

	Parameter	Value [a]
LIVOSTIN® Nasal Spray (Label Claim: 0.50 mg/mL)	Found (mg/mL), Mean (n = 5)	0.498
	Labeled amount found (%), Mean ± SD	99.60 ± 0.80
	RSD (%)	0.80
	Acceptance limits (% of labeled amount)[a]	90.0–110
	Compliance	Compliance

[a] Based on the manufacturer's general registered specification limits for the product, as no official compendial monograph for levocabastine nasal spray is currently available.

Table 5. Statistical comparison between the results of determination of pure levocabastine by the proposed method and the official method.

Parameters	Proposed Voltammetric Method	Official Method [a]
Mean	99.96	100.54
SD	0.38	1.05
n	5	5
Variance	0.15	1.11
t (2.306) [b]	1.16	—-
F (6.388) [b]	2.59	—-

[a] Official BP by volumetric titration method. [b] The values between parentheses are the corresponding theoretical values of *t* and F at a 95% confidence level.

3.6. Effect of the Co-Administered Drugs

We evaluated the selectivity of the developed sensor by examining its electrochemical response to LC in the presence of potential interfering substances, such as concurrently administered medications and common biological metabolites. AZE and EMD are second-generation antihistamines commonly prescribed alongside LC for the management of allergic rhinitis and conjunctivitis, respectively [44–47]. The simultaneous determination was performed using SWV in B-R buffer (pH 7.0) containing 2.0×10^{-6} M LC combined with equimolar concentrations (2.0×10^{-6} M) of AZE and EMD (Figure 8). The voltammograms exhibited distinct anodic peaks. In the LC-AZE mixture, peaks were observed at 0.65 V (LC) and 0.78 V (AZE), with a peak potential difference (ΔEp) of 130 mV. The LC-EMD mixture also exhibited peaks at 0.65 V (LC) and 0.96 V (EMD), with a potential difference of 310 mV. These substantial peak separations demonstrate that the CPE/MWCNT-CsCl/SDS sensor can precisely quantify LC even when these medications are administered concurrently or combined.

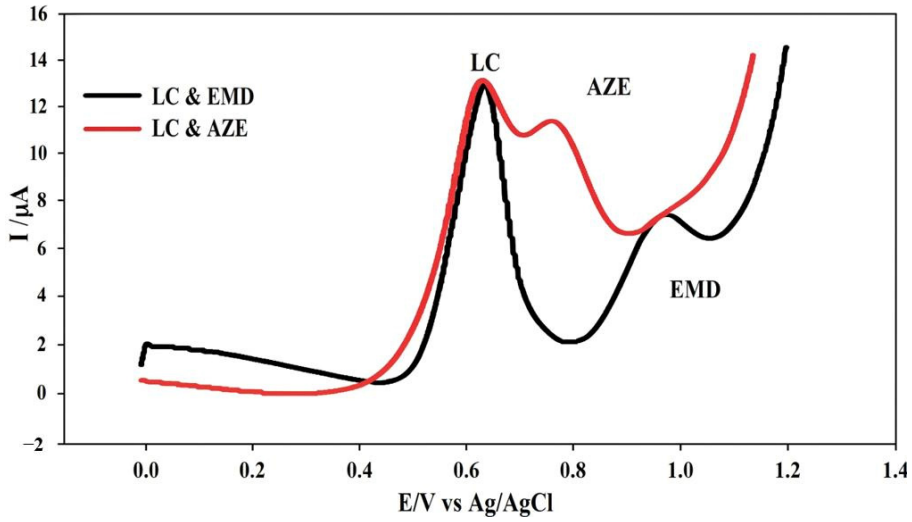


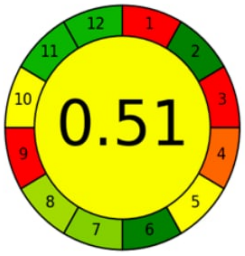
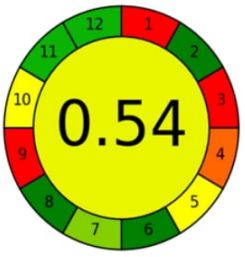
Figure 8. Square wave voltammograms for the simultaneous quantification of 2.0×10^{-6} M LC in the presence of 2.0×10^{-6} M AZE and EMD in B-R buffer (pH 7.0).

3.7. Comparative Evaluation and Green Assessment

In order to validate our proposed sensor against the previously reported methods for LC determination, a detailed comparison was conducted (Table 6). As observed, our sensor showed comparable sensitivity to the highly sensitive reported LC-MS/MS tech-

niques, in addition to the simplicity and fast analysis it offers. A green assessment was also carried out using the AGREE tool [48], and the proposed sensor obtained the highest score (0.79) among the compared methods (Table 6). It should be noted that the term "eco-friendly" refers to the overall analytical procedure rather than to the nanomaterial alone. This greenness is attributed to the following features: (i) the modifier is used in a small amount (5% composite in the carbon paste) and remains immobilized within the paste matrix, which is expected to limit its release; (ii) the sensor avoids the use of mercury-based electrodes; (iii) all measurements are carried out in aqueous buffer (5 mL) with minimal sample preparation (dilution and filtration) and without organic solvents during analysis, whereas the reported HPLC and LC-MS/MS methods require considerable volumes of organic solvents. Nevertheless, the nitric acid functionalization of MWCNTs, the use of diethyl ether during composite preparation, and the use of Nafion as a binder involve small quantities and are performed only once during sensor fabrication, and the long-term environmental fate of carbon nanotubes should be considered. Future work will explore greener functionalization routes and recyclable electrode materials.

Table 6. An overview of the reported methods for levocabastine determination, along with a green assessment.

Technique	LOD	Linear Range	Application	Green Assessment	Ref.
RP-HPLC	0.9 µg/mL	50–200 µg/mL	Stability-indicating in bulk drug and ophthalmic preparations		[9]
LC-MS/MS	0.003 µg/mL	0.05–0.5 µg/mL	In blood		[10]
LC-MS/MS	0.01 µg/mL	NA	In blood		[11]
Voltammetry	9.0×10^{-10} M ≈ 0.0004 µg/mL	5.0×10^{-9}–2.0×10^{-6} M	In bulk powder, pharmaceutical preparations, and artificial tears		This work

4. Conclusions

The first electroanalytical method for the determination of LC has been described. A sensor combining a MWCNTs/CsCl conductive network with an SDS film for electrostatic preconcentration and antifouling has been developed for this purpose. Structural and morphological characterizations validated the successful synthesis and synergistic assembly of the composite material. The beneficial amalgamation of MWCNT and Cs provided an electrocatalytic framework, while the addition of SDS enabled efficient preconcentration via electrostatic interactions. Electrochemical studies explained that the oxidation of LC is a diffusion-controlled, irreversible process involving the transfer of one electron and one proton. The proposed modified sensor exhibited good analytical performance, featuring a notably low detection limit and a wide linear dynamic range, superior to that of bare carbon paste electrodes. The sensor demonstrated significant resilience to co-administered drugs. Furthermore, the practical applicability of the suggested method was highlighted by its successful implementation in nasal spray and artificial tear samples, supporting its potential use in ocular pharmacokinetic studies.

Author Contributions: S.A.A. (Shimaa A. Atty): Conceptualization of the work, formal analysis, investigation, visualization of the data, methodology, validation, writing, review, and editing. S.M.A.: Writing—original draft, methodology, investigation, data curation. A.H.I.: Validation, investigation. F.A.F.: Writing—original draft, methodology, investigation, data curation. M.A.T.: Investigation, Resources, writing, review, and editing. S.A.A. (Suliman A. Almahmoud): Resources, writing, review, and editing. M.A.A.R.: Conceptualization of the work, formal analysis, investigation, visualization of the data, methodology, validation, writing, review, and editing. All authors have read and agreed to the published version of the manuscript.

Funding: The Researchers would like to thank the Deanship of Graduate Studies and Scientific Research at Qassim University (https://www.qu.edu.sa) for financial support (QU-APC-2026).

Institutional Review Board Statement: Not applicable.

Informed Consent Statement: Not applicable.

Data Availability Statement: The original contributions presented in this study are included in the article. Further inquiries can be directed to the corresponding author.

Acknowledgments: The Researchers would like to thank the Deanship of Graduate Studies and Scientific Research at Qassim University (https://www.qu.edu.sa) for financial support (QU-APC-2026). The authors would also like to acknowledge the use of Gemini 3.6 Flash (Google, Mountain View, CA, USA, 2026) for language polishing, text formatting, grammar checking, and refining the manuscript's clarity.

Conflicts of Interest: The authors declare no conflicts of interest.

Abbreviations

The following abbreviations are used in this manuscript:

CPE	Carbon paste electrode
MWCNTs	Multi-walled carbon nanotubes
SDS	Sodium dodecyl sulfate
LC	Levocabastine
CV	Cyclic voltammetry
SWV	Square wave voltammetry
AZE	Azelastine HCl
EMD	Emedastine difumarate

References

1. Scadding, G.K.; Kariyawasam, H.H.; Scadding, G.; Mirakian, R.; Buckley, R.J.; Dixon, T.; Durham, S.R.; Farooque, S.; Jones, N.; Leech, S.; et al. BSACI guideline for the diagnosis and management of allergic and non-allergic rhinitis (Revised Edition 2017; First edition 2007). *Clin. Exp. Allergy* **2017**, *47*, 856–889. [CrossRef] [PubMed]
2. Brunton, L.L.; Knollmann, B.C.; Hilal-Dandan, R. *Goodman & Gilman's the Pharmacological Basis of Therapeutics*; McGraw-Hill Education: New York, NY, USA, 2018; Volume 13.
3. Schata, M.; Jorde, W.; Richarz-Barthauer, U. Levocabastine nasal spray better than sodium cromoglycate and placebo in the topical treatment of seasonal allergic rhinitis. *J. Allergy Clin. Immunol.* **1991**, *87*, 873–878. [CrossRef] [PubMed]
4. Abelson, M.B.; Weintraub, D. Levocabastine Eye Drops: A New Approach for the Treatment of Acute Allergic Conjunctivitis. *Eur. J. Ophthalmol.* **1994**, *4*, 91–101. [CrossRef] [PubMed]
5. Fanelli, R.; Floquet, N.; Besserer-Offroy, E.l.; Delort, B.; Vivancos, M.l.; Longpré, J.-M.; Renault, P.; Martinez, J.; Sarret, P.; Cavelier, F. Use of Molecular Modeling to Design Selective NTS2 Neurotensin Analogues. *J. Med. Chem.* **2017**, *60*, 3303–3313. [CrossRef] [PubMed]
6. Brzezińska, E.; Kośka, G. A structure–activity relationship study of compounds with antihistamine activity. *Biomed. Chromatogr.* **2006**, *20*, 1004–1016. [CrossRef] [PubMed]
7. Hampel, F.C.; Martin, B.G.; Dolen, J.; Travers, S.; Karcher, K.; Holton, D. Efficacy and Safety of Levocabastine Nasal Spray for Seasonal Allergic Rhinitis. *Am. J. Rhinol.* **1999**, *13*, 55–62. [CrossRef] [PubMed]
8. Ghonim, R.; El-Awady, M.; Tolba, M.; Ibrahim, F. A comprehensive review of the analytical methods used for the determination of selected antihistamines in pharmaceutical dosage forms and biological fluids. *Delta Univ. Sci. J.* **2022**, *5*, 76–107. [CrossRef]
9. AlAani, H.; Alashkar, I.; Karabet, F. Development and validation of stability-indicating RP-HPLC method for the determination of Levocabastine HCl in bulk drug and in ophthalmic suspensions. *Arab. J. Chem.* **2017**, *10*, S3097–S3107. [CrossRef]
10. Gergov, M.; Robson, J.N.; Ojanperä, I.; Heinonen, O.P.; Vuori, E. Simultaneous screening and quantitation of 18 antihistamine drugs in blood by liquid chromatography ionspray tandem mass spectrometry. *Forensic Sci. Int.* **2001**, *121*, 108–115. [CrossRef] [PubMed]
11. Gergov, M.; Ojanperä, I.; Vuori, E. Simultaneous screening for 238 drugs in blood by liquid chromatography–ionspray tandem mass spectrometry with multiple-reaction monitoring. *J. Chromatogr. B* **2003**, *795*, 41–53. [CrossRef] [PubMed]
12. Hidalgo, J.; Turdean, G.L.; Falciola, L.; Pifferi, V.; Galambos, I.; Jankovics, H.; Toth, E.; Hidalgo, L. A functionalized multiwalled carbon nanotubes decorated with an engineered flagellin protein as a modified electrode for the detection of diclofenac sodium. *Microchem. J.* **2025**, *216*, 114698. [CrossRef]
13. Atty, S.A.; Abdel-raoof, A.M.; Fouad, F.A.; Mohamed, T.F.; Elbardisy, H.M. Green electrochemical methodology for simultaneous determination of atorvastatin and ezetimibe: Application to biological matrices. *Sustain. Chem. Pharm.* **2023**, *36*, 101300. [CrossRef]
14. Yehia, A.M.; Tantawy, M.A.; Farag, M.A.; Abdelshafi, N.A. A multichannel biosensor integrated with a controller board for standard addition voltammetric signal analysis of cardiac troponin-I. *Talanta* **2026**, *297*, 128661. [CrossRef] [PubMed]
15. Abbas, A.E.F.; Al-Khateeb, L.A.; Al Kamaly, O.; Tantawy, M.A.; Elyan, S.S. A nanocomposite electrochemical sensor for the first adsorption-controlled voltammetric sensing of pizotifen in pharmaceutical and biological matrices. *Microchem. J.* **2026**, *224*, 117802. [CrossRef]
16. Althobaiti, S.A.; Ahmed Gassmelseed Abdalla, D.; Tantawy, M.A.; Abbas, A.E.F. Avoiding rebound effects in green analysis: Comparative greenness and holistic sustainability assessment of a low-carbon electroanalytical method for the newly approved anti-anemia drug Desidustat. *Sustain. Chem. Pharm.* **2026**, *51*, 102419. [CrossRef]
17. Heragy, M.O.; Tantawy, M.A.; Moustafa, A.A.M.; Elghobashy, M.R.; El-Mosallamy, S.S. Molecularly imprinted metal-organic framework-based potentiometric sensor for sensitive detection of torsemide in dietary supplements and milk. *Food Chem.* **2026**, *517*, 149504. [CrossRef] [PubMed]
18. Rahman, M.A.A.; Saad, A.S.; El-Mosallamy, S.S.; Elghobashy, M.R.; Zaazaa, H.E.; Atty, S.A. Economical Voltammetric Sensor for Sensitive Rapid Determination of Ondansetron in the Presence of Opioid Antagonist Naltrexone. *Electrocatalysis* **2022**, *13*, 567–579. [CrossRef]
19. Atty, S.A.; Abdelzaher, A.M.; Barghash, S.; Rahman, M.A.A. Advanced screen-printed electrode functionalized ZnO/CNTs for the electrochemical analysis of opioid drug pethidine co administered with paracetamol: Application in dosage form and human plasma sample. *BMC Chem.* **2025**, *19*, 235. [CrossRef] [PubMed]
20. Tantawy, M.A.; El Fiky, H.A.; Badawey, A.M.; Abd El Ghany, M.F.; Fares, N.V. A Novel Glassy Carbon Electrode Modified with Multi-Walled Carbon Nanotubes for Potentiometric Xipamide Determination. *J. Electrochem. Soc.* **2021**, *168*, 056506. [CrossRef]
21. Sengupta, J.; Hussain, C.M. CNT and Graphene-Based Transistor Biosensors for Cancer Detection: A Review. *Biomolecules* **2023**, *13*, 1024. [CrossRef] [PubMed]
22. Islam, S.; Furuta, H. Recent Development of Carbon-Nanotube-Based Solar Heat Absorption Devices and Their Application. *Nanomaterials* **2022**, *12*, 3871. [CrossRef] [PubMed]

23. Vinoth, S.; Wang, S.-F. Construction of functionalized carbon nanotube@metal oxide nanocomposite for high-performance electrochemical measurement of antipyretic drug in water samples. *Environ. Sci. Pollut. Res.* **2024**, *31*, 46484–46497. [CrossRef] [PubMed]
24. Magar, H.S.; Duraia, E.-s.M.; Hassan, R.Y.A. Dopamine fast determination in pharmaceutical products using disposable printed electrodes modified with bimetal oxides carbon nanotubes nanocomposite. *Sci. Rep.* **2025**, *15*, 11229. [CrossRef] [PubMed]
25. Azab, S.M.; Fekry, A.M. A novel electrochemical determination for the anti-osteoporosis drug (alendronate sodium) and its application for corrosion monitoring of surgical 316 L SS bone implant. *J. Alloys Compd.* **2017**, *717*, 25–30. [CrossRef]
26. Bianco, A.; Kostarelos, K.; Prato, M. Applications of carbon nanotubes in drug delivery. *Curr. Opin. Chem. Biol.* **2005**, *9*, 674–679. [CrossRef] [PubMed]
27. Prato, M.; Kostarelos, K.; Bianco, A. Functionalized Carbon Nanotubes in Drug Design and Discovery. *Acc. Chem. Res.* **2007**, *41*, 60–68. [CrossRef] [PubMed]
28. Ferguson, W.; Gorrie, D. Cesium and Cesium Compounds. In *Kirk-Othmer Encyclopedia of Chemical Technology*; John Wiley & Sons: Hoboken, NJ, USA, 2011; pp. 1–17.
29. Sun, Q.; Zhang, G.; Tung, C.-H.; Wang, Y. Alkali Halide Cubic Cluster Anions ([Cs8X27]19–, X = Cl, Br) Isolated from Water. *Inorg. Chem.* **2016**, *55*, 11125–11130. [CrossRef] [PubMed]
30. Salama, N.N.; Zaazaa, H.E.; Azab, S.M.; Atty, S.A.; El-Kosy, N.M.; Salem, M.Y. A novel cesium modified carbon paste electrode for rapid selective determination of ropinirole in presence of co-administered and interference substances. *Sens. Actuators B Chem.* **2017**, *240*, 1291–1301. [CrossRef]
31. Atty, S.A.; Ibrahim, A.H.; Ibrahim, H.; Abdelzaher, A.M.; Abdel-Raoof, A.M.; Fouad, F.A. Simultaneous voltammetric detection of anti-depressant drug, sertraline HCl and paracetamol in biological fluid at CNT-cesium modified electrode in micellar media. *Microchem. J.* **2020**, *159*, 105524. [CrossRef]
32. Unal, D.N.; Sadak, S.; Erkmen, C.; Selcuk, Ö.; Uslu, B. Review of Surfactants, Structural Properties and Their Role in Electrochemistry. In *Surfactant-Based Sensors in Chemical and Biochemical Detection*; Manjunatha, J.G., Ed.; Royal Society of Chemistry: Cambridge, UK, 2023; Volume 23, pp. 1–18.
33. British Pharmacopoeia Commission. Commission, B.P., Ed.; *British Pharmacopoeia 2009*; Medicines and Healthcare Products Regulatory Agency (MHRA): London, UK, 2009.
34. Zhao, W.; Zhang, A.P.; Li, X.K.; Bian, J.; Yang, S.K.; Ni, K.Y.; Yang, K.C.; Lin, H.L.; Chen, D.Q. Novel flexible polyether segment polybenzoxazine shape memory nanocomposites reinforced by incorporating functionalized carbon nanotubes. *Compos. Part B Eng.* **2025**, *292*, 112104. [CrossRef]
35. Zhu, H.W.; Pan, Y.S.; Wang, Y.Q.; Xiang, Y.L.; Han, R.; Huang, R. Photocatalytic Activity and Antibacterial Properties of ZnO/CNTs Composites. *J. Nano Res.* **2024**, *82*, 55–75. [CrossRef]
36. Davies, J.A.; Mugglestone, M.; Yang, S.; Ellis, A.M. IR Spectroscopy of the Cesium Iodide–Water Complex. *J. Phys. Chem. A* **2020**, *124*, 6528–6535. [CrossRef] [PubMed]
37. Kittel, C.; McEuen, P.; McEuen, P. *Introduction to Solid State Physics*; Wiley: New York, NY, USA, 1976; Volume 8.
38. Laad, M.; Sur, A.; Kale, G.; Razoumny, Y.; Shalu, A. Synthesis and characterization of carbon based polymer composites reinforced with MWCNTs and graphite in PVDF matrix. *Sci. Rep.* **2025**, *15*, 28928. [CrossRef] [PubMed]
39. Fekry, A.M. A new simple electrochemical Moxifloxacin Hydrochloride sensor built on carbon paste modified with silver nanoparticles. *Biosens. Bioelectron.* **2017**, *87*, 1065–1070. [CrossRef] [PubMed]
40. Guidelli, R.; Compton, R.G.; Feliu, J.M.; Gileadi, E.; Lipkowski, J.; Schmickler, W.; Trasatti, S. Defining the transfer coefficient in electrochemistry: An assessment (IUPAC Technical Report). *Pure Appl. Chem.* **2014**, *86*, 245–258. [CrossRef]
41. Schäfer, H.-J. Recent contributions of kolbe electrolysis to organic synthesis. In *Proceedings of the Electrochemistry IV*; Springer: Berlin/Heidelberg, Germany, 1990; pp. 91–151.
42. Leech, M.C.; Lam, K. Electrosynthesis Using Carboxylic Acid Derivatives: New Tricks for Old Reactions. *Acc. Chem. Res.* **2020**, *53*, 121–134. [CrossRef] [PubMed]
43. Atty, S.A.; Abdallah, O.M.; Abdelrahman, M.A.; Abdel-Megied, A.M. A Newly Developed Electrochemical Method for the Simultaneous Determination of Camylofin and Analgine in Pharmaceutical Preparation and Biological Fluids. *J. Electrochem. Soc.* **2019**, *166*, B1217. [CrossRef]
44. Tantilipikorn, P.; Kirtsreesakul, V.; Bunnag, C.; Vangveeravong, M.; Thanaviratananich, S.; Chusakul, S. The Use of Azelastine Hydrochloride/Fluticasone Propionate in the Management of Allergic Rhinitis in Asia: A Review. *J. Asthma Allergy* **2024**, *17*, 667–679. [CrossRef] [PubMed]
45. Leonardi, A.; Quintieri, L.; Presa, I.J.; Lloves, J.M.; Montero, J.; Benítez-del-Castillo, J.M.; Lestón, F.J.S.; González-Mancebo, E.; Asero, R.; Groblewska, A.; et al. Allergic Conjunctivitis Management: Update on Ophthalmic Solutions. *Curr. Allergy Asthma Rep.* **2024**, *24*, 347–360. [CrossRef] [PubMed]
46. Falser, N.; Wolfgang, W.; Rahlfs, V.W.; Baehre, M. Comparative Efficacy and Safety of Azelastine and Levocabastine Nasal Sprays in Patients with Seasonal Allergic Rhinitis. *Arzneimittelforschung* **2001**, *51*, 387–393. [CrossRef] [PubMed]

47. Giede, C.; Metzenauer, P.; Petzold, U.; Ellers-Lenz, B. Comparison of Azelastine Eye Drops with Levocabastine Eye Drops in the Treatment of Seasonal Allergic Conjunctivitis. *Curr. Med. Res. Opin.* **2000**, *16*, 153–163. [CrossRef]
48. Pena-Pereira, F.; Wojnowski, W.; Tobiszewski, M. AGREE—Analytical GREEnness Metric Approach and Software. *Anal. Chem.* **2020**, *92*, 10076–10082. [CrossRef] [PubMed]

Disclaimer/Publisher's Note: The statements, opinions and data contained in all publications are solely those of the individual author(s) and contributor(s) and not of MDPI and/or the editor(s). MDPI and/or the editor(s) disclaim responsibility for any injury to people or property resulting from any ideas, methods, instructions or products referred to in the content.